POLITECNICO DI TORINO
Repository ISTITUZIONALE

Gearshift control strategies for hybrid electric vehicles: A comparison of powertrains equipped with automated manual transmissions and dual-clutch transmissions

Original
Gearshift control strategies for hybrid electric vehicles: A comparison of powertrains equipped with automated manual transmissions and dual-clutch transmissions / Guercioni, GUIDO RICARDO; Vigliani, Alessandro. - In: PROCEEDINGS OF THE INSTITUTION OF MECHANICAL ENGINEERS. PART D, JOURNAL OF AUTOMOBILE ENGINEERING. - ISSN 0954-4070. - STAMPA. - 233:11(2019), pp. 2761-2779. [10.1177/0954407018804120]

Availability:
This version is available at: 11583/2715010 since: 2019-09-07T09:43:30Z

Publisher:
LONDON:SAGE PUBLICATIONS LTD

Published
DOI:10.1177/0954407018804120

Terms of use:

This article is made available under terms and conditions as specified in the corresponding bibliographic description in the repository

Publisher copyright
Sage postprint/Author's Accepted Manuscript

Guercioni, GUIDO RICARDO; Vigliani, Alessandro, Gearshift control strategies for hybrid electric vehicles: A comparison of powertrains equipped with automated manual transmissions and dual-clutch transmissions, accepted for publication in PROCEEDINGS OF THE INSTITUTION OF MECHANICAL ENGINEERS. PART D, JOURNAL OF AUTOMOBILE ENGINEERING (233 11) pp. 2761-2779. © 2019

(Article begins on next page)

12 October 2024

Gearshift Control Strategies for HEVs: a Comparison of Powertrains Equipped with AMTs and DCTs

Journal:	*Part D: Journal of Automobile Engineering*
Manuscript ID	JAUTO-18-0151.R1
Manuscript Type:	Original Article
Date Submitted by the Author:	n/a
Complete List of Authors:	Guercioni, Guido; Politecnico di Torino, Dipartimento di Ingegneria Meccanica e Aerospaziale Vigliani, Alessandro; Politecnico di Torino, Dipartimento di Ingegneria Meccanica e Aerospaziale
Keywords:	hybrid vehicles, Transmission, Vehicle powerline, Dual Clutch Transmission (DCT), Automated Manual Transmissions (AMT), Gearshift Control, Drive quality
Abstract:	This paper describes gearshift control strategies developed for a series-parallel Hybrid Electric Vehicle (HEV) architecture in which an electric machine is connected to the output of the transmission, thus obtaining torque filling capabilities during gearshifts. Two transmission systems are analyzed: Hybrid Automated Manual Transmission (H-AMT) and Hybrid Dual-Clutch Transmission (H-DCT). The paper focuses on the gearshift control strategies for the two transmission, splitting each gearshift into several phases. The objectives of each control phase, the equations for computing the set points for powertrain actuators and the conditions that determine the passage from one shifting phase to the next are reported. Moreover, nonlinear dynamic models are described and used to verify through simulation the effectiveness of the controllers. Promising results, in terms of vehicle dynamic performance, are obtained for both transmission systems.

SCHOLARONE™
Manuscripts

For Peer Review

Original Article

Corresponding Author:
Alessandro Vigliani, Dipartimento di Ingegneria Meccanica e Aerospaziale, Politecnico di Torino, Corso Duca degli Abruzzi 24, 10129 Torino, Italy.
Email: alessandro.vigliani@polito.it

Gearshift Control Strategies for HEVs: A Comparison of Powertrains Equipped with AMTs and DCTs

Abstract

This paper describes gearshift control strategies developed for a series-parallel Hybrid Electric Vehicle (HEV) architecture in which an electric machine is connected to the output of the transmission, thus obtaining torque filling capabilities during gearshifts. Two transmission systems are analyzed: Hybrid Automated Manual Transmission (H-AMT) and Hybrid Dual-Clutch Transmission (H-DCT). The paper focuses on the gearshift control strategies for the two transmission, splitting each gearshift into several phases. The objectives of each control phase, the equations for computing the set points for powertrain actuators and the conditions that determine the passage from one shifting phase to the next are reported. Moreover, nonlinear dynamic models are described and used to verify through simulation the effectiveness of the controllers. Promising results, in terms of vehicle dynamic performance, are obtained for both transmission systems.

Keywords

Hybrid Electric Vehicle (HEV), Dual Clutch-Transmission (DCT), Automated Manual Transmissions (AMT), Gearshift Control, Drive quality.

Guido R. Guercioni and Alessandro Vigliani

Dipartimento di Ingegneria Meccanica e Aerospaziale, Politecnico di Torino, Torino, Italy.

Introduction

The increasing demand seen in the last few years for improved vehicle dynamic performance and reduced fuel consumption has raised the interest of automotive industry to explore new powertrain technologies.
The electrification of powertrain systems provides energy efficiency benefits since it enables the possibility of performing regeneration during braking and engine downsizing ([1]). Furthermore, the presence of an extra power generation device enables improvements in the overall vehicle performance ([2]). However, these benefits can be fully exploited only if the system is properly controlled.

For Peer Review

Dual-Clutch Transmissions (DCTs) ([3, 4]) are good candidates to be integrated into Hybrid Electric Vehicle (HEV) powertrain architectures since they allow high efficiency, similar to Manual Transmissions (MTs) ([5]) or Automated Manual Transmissions (AMTs) ([6]) and almost seamless gearshift operations with a high tunability. This is achieved at the expense of increased mechanical complexity.

Several previous studies have investigated gearshift quality for conventional DCTs ([7–10]) and MTs/AMTs ([11–13]) using a series of different metrics. Furthermore, research efforts also focused on exploring the integration of Electric Machines (EMs) into powertrains equipped with the mentioned transmission systems, aiming at improving vehicle performance ([2, 14 and 15]).

Among the different HEV architectures currently available, attention has been drawn to the possibility of connecting an EM to the transmission output shaft: this configuration enables full or partial compensation of torque gap during gearshifts, if the EM torque is properly controlled ([15, 16]). In [2], an upshift control strategy is developed for a hybridized MT in which the torque gap is successfully reduced thanks to the intervention of the EM. This controller could also be applied for hybrid powertrains equipped with AMTs. Moreover, improvements in terms of drive comfort can be achieved, as visible when the comparing the performance of a Hybrid Dual-Clutch Transmission (H-DCT) to that of a conventional DCT ([17]).

Regarding the smoothness of the clutch re-engagement process, [18] analytically proves that the oscillations of the longitudinal vehicle acceleration generated at the clutch engagement, depend on the slip speed and acceleration at the clutch lock-up. Based on these considerations, a variety of control strategies have been proposed to reduce vibrations when the oncoming clutch is engaged using different techniques. For example, in [12] a solution based on cascaded and decoupled speed and torque control loops is proposed for a conventional AMT. In [15], an optimal controller for the clutch re-engagement phase performed with a Hybrid Automated Manual Transmission (H-AMT) is discussed. The control algorithm is based on the augmentation of the reference trajectories, resulting into a homogeneous TPBVP (Two-Point Boundary-Value Problem). Moreover, a control strategy for a H-DCT is presented in [19]: the characteristics of a robust H_∞ controller are exploited to complete the speed synchronization of the Internal Combustion Engine (ICE) and the clutch driven plate. Moreover, energy dissipation in the form of heat during clutch slip should be limited, thus reducing fuel consumption and increasing component life. Several control algorithms with the objective of minimizing this energy dissipation during gearshift maneuvers can be found in literature for both conventional and hybrid powertrains ([15, 20]).

In the present work, control algorithms for upshift and downshift maneuvers are developed for a series-parallel Hybrid Electric Vehicle (HEV) architecture in which an EM is connected to the output of the transmission. Two different control logics are developed for the same vehicle depending on the type of transmission under analysis: AMT or DCT. The proposed strategies are very simple to implement and tune since they are based on simple Proportional-Integral (PI) feedback controllers.

For the assessment of gearshift quality, nonlinear dynamic models are designed to properly simulate the longitudinal vehicle dynamics with the objective of developing a

For Peer Review

tool that can be used both for control calibration and drivability assessment. Examples of nonlinear dynamic models can be found in [4, 15 and 21].
The results obtained for both powertrains are promising in terms of vehicle performance. It is of interest underlining that the H-AMT studied has proved capable of almost eliminating the torque gap during gearshifts while keeping the mechanical complexity of the system low with respect to its DCT counterpart. Since some H-DCTs are already on the market, a comparison between these two transmission systems becomes of interest. Furthermore, the authors are not aware of any study regarding an effective comparison of H-AMTs and H-DCTs performance, therefore, this topic is explored here.
The present paper is organized as follows. In section 2, the model is addressed, while in section 3, the metrics employed for gearshift quality assessment are discussed. Section 4 illustrates how the driver inputs are processed to generate a torque request at the wheels. Then, in the following three sections, gearshift control strategies for the two variants of the HEV of interest are discussed. The objectives of each control phase, the equations for computing the set points to powertrain actuators and the conditions that determine the passage from one shifting phase to the next are reported. Finally, simulation results are presented and analyzed to illustrate the effectiveness of the control strategies.

Vehicle powertrain

Powertrain description

The vehicle studied presents the series-parallel HEV architecture shown in Figure 1. The powertrain consists of an ICE, a Belt Alternator Starter (BAS), an EM, a battery pack and a mechanical transmission system. Two variants of this powertrain are studied, the main difference between them is in the type of transmission employed: AMT or DCT.
The EM is connected to the driveshaft through a mechanical coupler referred to as Power Transfer Unit (PTU). A single gear ratio is available to the electric motor. This configuration enables full or partial compensation of the torque gap during gearshifts. Moreover, as it is typical of hybridized powertrains, the introduction of the EM enables the possibility of performing regenerative braking.
In addition to the EM connected to the transmission output, a BAS is employed to use electrical power to support the ICE in delivering the requested torque. Due to its fast response, the BAS helps in improving the control of the ICE speed during gearshifts ([22]).
"[Insert Figure 1.]"

Figure 1. Powertrain layout.

To filter torsional vibrations, a Single Mass Flywheel (SMF) is located between the ICE and the clutch (or dual-clutch unit for the DCT variant). In addition, torsional dampers are incorporated into each clutch.
The proposed HEV architecture enables the possibility of operating in several different modes. In order to obtain the highest possible tractive force at the wheels, BAS, ICE and EM can be used together to propel the vehicle, thus operating in parallel hybrid mode. Note that the ICE can produce additional power with respect to that required at the wheels, in this case, the EM or the BAS could use this extra energy to recharge the

For Peer Review

battery. On the other hand, the transmission systems considered allow to disconnect the ICE from the wheels. This enables the possibility of driving the vehicle in either series hybrid mode or EV-mode without having to drag the ICE inertia and compensate for its energy losses. In particular, the powertrain operates as a series hybrid when the ICE is used to charge the battery through the BAS and the EM provides the power requested at the wheels. The principal components specifications are shown in Table 1.

Table 1. Powertrain specifications.

Component	Data
Vehicle mass	1920 kg
ICE	Diesel engine, 2.0 L, 104 kW
EM	112 kW (peak power)
BAS	32 kW (peak power)
DCT or AMT	6-speed transmission
Battery Pack	Li-ion, 18.9 kWh

For Peer Review

Powertrain model

For the assessment of gearshift quality and its impact on drivability in powertrains with DCTs and AMTs, nonlinear dynamic models are required; note that gearshift quality criteria will be described later. They must be able to deal with the change in the number of Degrees Of Freedom (DOF) due to variations in the clutch status (engaged/disengaged) or in the synchronizers position. Furthermore, the models should be able to properly account for the driveline components compliance and damping. In this way, the first torsional mode of the transmission is correctly estimated and an assessment of the vehicle drivability during gearshift maneuvers can be exploited ([11]).
A global layout of the model developed of the powertrain variant in which an AMT is employed can be seen in Figure 2.
"[insert Figure 2]"

Figure 2. Powertrain model: AMT.

Figure 3 illustrates the structure of the model developed for the powertrain variant with DCT.
"[insert Figure 3]"

Figure 3. Powertrain model: DCT.

The DCT model has a structure similar to the one developed for the AMT variant, the main difference being an additional transmission path to consider.

Note that the variables related to the transmission path in which the oncoming gear is located will be identified with subscript n, while for those related to the transmission path in which the offgoing gear is mounted, subscript pr is employed.
A summary of the main model inputs is presented below for the two powertrains:
oncoming and offgoing gear number;
initial angular position and speed of each DOF;
ICE, BAS and EM torque request;
oncoming and offgoing clutch transmissible torque request;
synchronizer position request (only for the AMT variant).
Instead, the main model outputs correspond to the angular position and speed of each DOF.
The models used for each powertrain component are described in the following paragraphs.

ICE

The engine shaft dynamics is described by:

$$T_{ICE,eq}(t) - T_c(t) = J_{ICE,eq}\dot{\omega}_{ICE}(t) \quad (1)$$

$$J_{ICE,eq} = J_{ICE} + J_{SMF} + J_{cm} + J_{BAS}\tau_{BAS}^2 \quad (2)$$

where $T_{ICE,eq}(t)$ is the sum of the ICE and BAS torque and $\dot{\omega}_{ICE}(t)$ is the angular acceleration of the crankshaft. Moreover, J_{ICE}, J_{SMF}, J_{cm} and J_{BAS} are respectively the inertia of the ICE, SMF, clutch mechanism and BAS inertia. τ_{BAS} is the transmission ratio of the belt connecting the BAS to the crankshaft.
The torque transmitted through clutch $T_c(t)$ (or dual-clutch unit for the DCT variant) is computed using a LuGre dynamic friction model ([23, 24]). This dynamic model allows to simulate different friction regimes, i.e., pre-sliding and sliding, without requiring any switching functions. In particular, as opposed to static models, LuGre formulation accounts for the small pre-sliding displacements that occur in standstill friction conditions at which the friction force is a function of displacement ([24]).
The physical limitations on torque and speed for ICE and BAS are considered. The maximum and minimum torque that can be provided by these components are expressed as a function of the crankshaft angular speed.

Clutch damper

A torsional damper is incorporated in each clutch; modeled as a two-stage damper with piecewise linear stiffness and hysteresis.
The spring element generates restoring torque $T_{tds,pr}(t)$ based on stiffness $k_{td}(t)$ that is a function of the angular position difference between the DOF corresponding to the clutch disc (located before the damper) and the primary shaft $\theta_{cd,j}(t) - \theta_{p,j}(t)$.
Therefore, for the offgoing gear transmission path:

$$T_{tds,pr}(t) = k_{td}(t)\left(\theta_{cd,pr}(t) - \theta_{p,pr}(t)\right) \quad (3)$$

On the other hand, the energy dissipation introduced by the clutch damper is modeled using a Coulomb friction model (smoothed through a hyperbolic tangent function) ([23]) based on the clutch damper hysteresis $T_{o,tdh}(t)$ which is also a function of $\theta_{cd,j}(t) - \theta_{ps,j}(t)$:

$$T_{tdh,pr}(t) = T_{o,tdh}(t)\, tanh\left(3\frac{\omega_{cd,pr}(t) - \omega_{p,pr}(t)}{\Delta\omega_{th,td}}\right) \quad (4)$$

The total torque transmitted by the clutch damper is then:

$$T_{td,pr}(t) = T_{tds,pr}(t) + T_{tdh,pr}(t) \quad (5)$$

Finally, the dynamic equation of the clutch is:

$$T_c(t) - T_{td,pr}(t) = J_{cd,pr,1}\dot{\omega}_{cd,pr}(t) \quad (6)$$

where $J_{cd,pr,1}$ is the inertia of the clutch disc (part of its total inertia located before the damper) and $\dot{\omega}_{cd,pr}$ is the angular acceleration of the clutch disc.
The clutch damper torque and the clutch disc dynamics for the transmission path related to the oncoming gear, $T_{td,n}(t)$ and $\dot{\omega}_{cd,n}(t)$, are computed in a similar manner. Note that for the AMT variant, the subscripts n and pr are not needed for these variables since there is only one clutch damper and gearbox input shaft (see Figure 2).

AMT and EM

A stick diagram of the AMT is visible in Figure 4. The transmission is composed of:
a dry clutch;
an input/primary shaft;
two output/secondary shafts (upper and lower) that are linked to the differential ring gear via pinion gears;
synchronizers mounted on the secondary shafts.

Note that the reverse gear is not represented in the figure.

The primary shaft dynamics can be described by:

$$T_{td}(t) - T_{pb}(t) - \frac{T_{syn}(t)}{\tau_{GB}(t)} = J_{p,eq}\dot{\omega}_p(t) \quad (7)$$

$$J_{p,eq} = J_p + J_{cd,2} \quad (8)$$

where J_p and $J_{cd,2}$ are respectively the inertia of the primary shaft and the clutch disc (portion located after the damper). $\tau_{GB}(t)$ is the transmission ratio according to the engaged gear.
"[insert Figure 4.]"

Figure 4. AMT schematic layout.

The bearings that support the transmission shafts introduce a torque loss (namely $T_{pb}(t)$ for the primary shaft, $T_{sb,pr}(t)$ and $T_{sb,n}(t)$ for the secondary shafts and $T_{db}(t)$ for the differential) computed as the sum of two contributions: Coulomb friction (computed similarly to the friction losses of the clutch damper) and viscous damping.
To model the torsional dynamics of the synchronizers a switching model is developed: whenever a gear is engaged, the synchronizer is considered as a gear mesh. During the synchronization of the speed of input and output shaft, the synchronizer is modeled as a friction element.
The torque transmitted through the synchronizers when a gear is engaged is computed considering constant contact stiffness k_{syn} and damping c_{syn}:

$$T_{syn}(t) = k_{syn}\left(\frac{\theta_p(t)}{\tau_{GB}(t)} - \theta_s(t)\right) + c_{syn}\left(\frac{\omega_p(t)}{\tau_{GB}(t)} - \omega_s(t)\right) \quad (9)$$

For Peer Review

where $\theta_s(t)$ and $\omega_s(t)$ are the angular position and speed of the secondary shaft. As mentioned before, the flexibility of transmission shafts is neglected, thus implying that the motion of both secondary shafts is the same.
During the synchronization of primary and secondary shafts, that occurs each time a new gear is to be engaged, the torque passing through the synchronizer is computed using a dynamic LuGre friction model ([23, 24]). Note that for the AMT, it is obviously assumed that only one synchronizer can be transmitting torque.
The equation governing the secondary shaft motion is:

$$T_{syn}(t) + T_{EM}(t)\tau_{EM} - T_{sb}(t) - \frac{T_{db}(t)}{\tau_d} - 2\frac{T_{hs}(t)}{\tau_d} = J_{s,eq}\dot{\omega}_s(t) \qquad (10)$$

where

$$T_{sb}(t) = T_{sb,pr}(t) + T_{sb,n}(t) \qquad (11)$$

$$J_{s,eq} = J_{s,pr} + J_{s,n} + J_{EM}\tau_{EM}^2 + J_{PTU} + \frac{J_d}{\tau_d^2} \qquad (12)$$

$T_{EM}(t)$ is the torque provided by the EM. $T_{hs}(t)$ is the half-shaft torque. $J_{s,j}, J_{EM}, J_{PTU}$, and J_d are the inertias of the secondary shafts, EM, PTU and differential. τ_{EM} is the transmission ratio provided by the PTU and τ_d is the final ratio.
As for the ICE, the maximum and minimum values of the EM torque are expressed as a function of the angular speed.

DCT and EM

A stick diagram of the DCT is visible in Figure 5. This transmission system is composed of:
a Dual-Clutch Unit (DCU) composed of dry clutches;
two concentric input/primary shafts (the inner one, carrying the odd driving gears, and the outer one the even driving gears);
two output/secondary shafts (upper and lower) that are linked to the differential ring gear via pinion gears;
synchronizers mounted on the secondary shafts.

Note that the reverse gear is not represented in the figure.
The two layouts shown in Figure 5 and Figure 4 are similar, due to the fact that the DCT here presented was designed starting from the AMT. The fact that one transmission is derived from the other provides the opportunity of making a fairer comparison. Since several components are similar, differences in the vehicle performance are likely to be related to the functioning principle of each transmission technology rather than to the components.
The dynamics of the primary shaft related to the offgoing gear can be described as:

$$T_{td,pr}(t) - T_{pb,pr}(t) - T_{pbr}(t) - \frac{T_{syn,pr}(t)}{\tau_{pr}(t)} = J_{p,pr,eq}\dot{\omega}_{p,pr}(t) \qquad (13)$$

$$J_{p,pr,eq} = J_{p,pr} + J_{cd,pr,2} \qquad (14)$$

where $T_{pbr}(t)$ is the torque loss introduced by the bearings located between the primary shafts, $\tau_j(t)$ is the transmission ratio of the DCT and $J_{cd,j,2}$ is the inertia of the clutch disc (part of its total inertia located after the damper). For the primary shaft where the oncoming is mounted, a similar expression is used.
"[insert Figure 5.]"

For Peer Review

Figure 5. DCT schematic layout.

Since the synchronizers of the current and oncoming gear are assumed to be engaged before the gearshift maneuver starts, a friction model is not needed for these components as it was necessary for the AMT variant. Hence, the synchronizers are modeled as a gear mesh with constant stiffness and damping (see Eq. (9)).
The equation governing the secondary shaft motion is:

$$T_{syn,pr}(t) + T_{syn,n}(t) + T_{EM}(t)\tau_{EM} - T_{sb}(t) - \frac{T_{db}(t)}{\tau_d} - 2\frac{T_{hs}(t)}{\tau_d} = J_{s,eq}\dot{\omega}_s(t) \quad (15)$$

$$J_{s,eq} = J_{s,pr} + J_{s,n} + J_{EM}\tau_{EM}^2 + J_{PTU} + \frac{J_d}{\tau_d^2} \quad (16)$$

Half-shafts

The half-shafts are simply modelled as linear stiffness and damping elements:

$$T_{hs}(t) = k_{hs}\left(\frac{\theta_s(t)}{\tau_d} - \theta_w(t)\right) + c_{hs}\left(\frac{\omega_s(t)}{\tau_d} - \omega_w(t)\right) \quad (17)$$

where k_{hs} and c_{hs} are the equivalent stiffness and damping coefficients, $\theta_w(t)$ and $\omega_w(t)$ are the angular position and speed of the driving wheels respectively. Note that for simplicity, the motion of the right and left wheel on the same axle is considered to be the same.

Wheels

The developed model has a DOF for each wheel. Pacejka'96 transient nonlinear tire model ([25]) is used to compute the longitudinal forces exchanged at the wheel/road contact. Hence, the dynamics of a single driving wheel is given by:

$$T_{hs}(t) - F_{x,Dr}(t)r_w - T_{rr,Dr}(t) = J_w\dot{\omega}_{w,Dr}(t) \quad (18)$$

while for the driven wheels it holds:

$$F_{x,dr}(t)r_w - T_{rr,dr}(t) = J_w\dot{\omega}_{w,dr}(t) \quad (19)$$

where $F_{x,Dr}$ and $F_{x,dr}$ are the outputs of the tire model. $T_{rr,Dr}$ and $T_{rr,dr}$ are the rolling resistance torques for each wheel, $\dot{\omega}_{w,Dr}$ and $\dot{\omega}_{w,dr}$ are the angular acceleration of the driving and driven wheels respectively. J_w is the inertia of a single wheel and r_w is the tire radius.
The rolling resistance torque can be calculated as:

$$T_{rr,j}(t) = F_{z,j}(t)\left(c_{0,rr} + c_{1,rr}\frac{v^2(t)}{r_w^2}\right) \quad (20)$$

where $c_{0,rr}$ and $c_{1,rr}$ are the rolling resistance coefficients. $v(t)$ is the vehicle longitudinal speed and $F_{z,j}(t)$ is the vertical load acting on the tire. Longitudinal load transfer for the estimation of the instantaneous tire vertical load is also considered.

Vehicle road load

The vehicle possesses only one DOF, corresponding to longitudinal motion. The vehicle longitudinal dynamics is given by:

$$2F_{x,Dr}(t) - 2F_{x,dr}(t) - F_{aer}(t) - F_g(t) = Ma(t) \quad (21)$$

where M is the vehicle mass, a is its longitudinal acceleration, F_{aer} is the aerodynamic drag force and F_g is the road grade force.
The aerodynamic drag force is computed as a quadratic function of the vehicle speed:

For Peer Review

$$F_{aer}(t) = \frac{1}{2}\rho_{aer}A_v c_{aer} v^2(t) \tag{22}$$

where ρ_{aer} is the air density, A_v is the vehicle frontal area and c_{aer} is the aerodynamic drag coefficient.
For the grade force it holds:

$$F_g(t) = Mg\ sin\big(\alpha(t)\big) \tag{23}$$

where $\alpha(t)$ is the road grade angle. Since the road is assumed to be flat the gravitational force F_g is zero.

Metrics for gearshift quality assessment

The metrics employed to assess gearshift quality are selected to allow an objective evaluation of the developed control strategies performance in terms of vehicle drivability and energy consumption.

Shift comfort

Generally speaking, longitudinal acceleration is the main parameter used to evaluate vehicle drivability. During gearshifts, the vehicle longitudinal acceleration variation should be as smooth as possible. Hence, the metric used to judge drive comfort will be jerk, *i.e.*, the derivative of acceleration ([26]), as done in [11, 17]. When evaluating vehicle drivability using its longitudinal acceleration, the usual practice is to only consider frequencies equal or lower than 10 Hz ([27]). This can be justified by the fact that the different parts of the human body have resonant frequencies in the 1 to 10 Hz range ([28]).
Based on the previous considerations, a filter is applied to the vehicle longitudinal acceleration before computing jerk. The filter used is a 3rd order lowpass digital Butterworth filter with a cutoff frequency of 10 Hz.
The Jerk RMS (Root Mean Square) value has been used in several studies to evaluate the effects of gearshift control strategies on vehicle drivability ([14, 19]). This parameter can be computed as:

$$Jerk_{RMS}(t) = \sqrt{\frac{1}{t_f}\int_{t_0}^{t_f} Jerk^2(t)\, dt} \tag{24}$$

In addition, another parameter used is the maximum and minimum jerk peak difference during the entire gearshift process ([11]), i.e.:

$$Jerk_{max/min} = Jerk_{max} - Jerk_{min} \tag{25}$$

Vehicle performance

In terms of vehicle performance, it is desirable to complete the gearshift maneuver as fast as possible while satisfying the torque request expressed by the driver. Hence, three parameters are considered to assess the vehicle performance:
gearshift duration: t_{gs};
mean vehicle longitudinal acceleration: $\bar{a}$;

For Peer Review

mean torque error: $\bar{T}_{w,err}$.

To quantify how well the torque request is satisfied, the absolute difference between the requested torque and the total torque at the transmission output is computed as a percentage of the torque request. i.e.:

$$T_{w,err}(t) = \left|\frac{T_{w,rq}(t) - T_{w,tot}(t)}{T_{w,rq}(t)}\right| 100 \tag{26}$$

where $T_{w,rq}(t)$ is the torque request at the wheels and $T_{w,tot}(t)$ is the total torque at the transmission output.

Note that high T_{err} is inversely proportional to performance. To assess gearshift performance, the mean value is used.

The total torque at the gearbox output reported at the wheels must be computed differently for each transmission layout. For the AMT, it holds:

$$T_{w,tot}(t) = \left(T_c(t)\tau_{GB}(t) + T_{syn}(t) + T_{EM}(t)\tau_{EM}\right)\tau_d \tag{27}$$

whereas, for the DCT variant it yields:

$$T_{w,tot}(t) = \left(\sum_j T_{c,j}(t)\,\tau_j + T_{EM}(t)\tau_{EM}\right)\tau_d \tag{28}$$

Shift efficiency

As mentioned before, energy dissipation during clutch slip should be limited to reduce fuel consumption and increase component life. In the present work, the total clutch energy loss is considered as a parameter to assess shift efficiency. The energy dissipated by the clutches is computed as the integral of the power loss:

$$E_{c,dis}(t) = \int_{t_0}^{t_f} \sum_j T_{c,j}(t)\omega_{cs,j}(t)\,dt \tag{29}$$

where $\omega_{cs,j}(t)$ is the clutch angular slip velocity. Note that this parameter is also a measure of durability (clutch wear).

Torque fill energy consumption

It was noticed in simulation that a variable related to the differences between the two powertrain variants is the mechanical energy required from the EM to satisfy the torque request at the wheels, i.e.:

$$E_{EM}(t) = \int_{t_0}^{t_f} T_{EM}(t)\omega_{EM}(t)\,dt \tag{30}$$

where $\omega_{EM}(t)$ is the EM angular speed.

Torque request during gearshifts

If the engine does not deliver as much power as expected, this is perceived by the driver as a symptom of poor vehicle drivability ([29]). During gearshift maneuvers, the torque delivered to the wheels should reflect the driver's intentions expressed in terms of the Accelerator Pedal Position (APP) ([19]). Hence, the torque request at the wheels is:

For Peer Review

$$T_{w,rq}(t) = T_n(t)\tau_n\tau_d \quad (31)$$

where $T_n(t)$ corresponds to the torque that would be provided by the ICE if the requested gear was already engaged.

The Engine Control Unit (ECU) receives a percentage based torque request and processes this input to generate the actual torque request ([30]), i.e.:

$$T_n(t) = ICE_{map}(APP(t), \omega_s(t)\tau_n) \quad (32)$$

The variable ICE_{map} is a stationary torque map in which the output is a function of the APP and crankshaft speed.

The transition between the torque request at the wheels computed considering the transmission ratio of the offgoing gear and the one determined in Eq. (31) is smoothed by means of a first order transfer function. Note that the value of the time constant could be adjusted to modify the trade-off between powertrain responsiveness and jerk intensity.

Gearshift control for HEV powertrains equipped with AMTs

As for all the gearshift control strategies presented in this paper, the algorithm developed for H-AMT is designed aiming at reducing as much as possible the oscillations in the vehicle longitudinal acceleration while satisfying the driver's torque request in the shortest possible time.

The controller design in this study is carried out separating the entire gearshift process into six consecutive phases in analogy with what it is shown in [12] and [11] for a traditional AMT and a TGF-AMT respectively. The gearshift phases are (see Figure 7):

Phase I: Go-to-slip.
Phase II: Opening the clutch completely.
Phase III: Disengage current gear / Speed synchronization / Engage new gear.
Phase IV: Prepare to start closing the clutch.
Phase V: Clutch slip control for engagement.
Phase VI: Close the clutch completely.

Exit conditions for each of these phases are established and used to switch between consecutive phases.

The designed controller relies only on speed measurements that are usually available in automated commercial vehicles:

ICE angular speed;
transmission input shaft angular speed;
transmission output shaft angular speed.

The controller output signals are:

torque request to EM;
torque request to ICE;
clutch transmissible torque request;
synchronizer position request.

In order to satisfy the request to the ICE, the BAS will produce the maximum torque; the remaining power necessary to fulfill the request will be supplied by the ICE. In addition, the clutch transmissible torque request is translated into a position command for the clutch actuator. Instead, a synchronizer position request will trigger the intervention of

For Peer Review

the low-level controllers responsible for either disengaging the offgoing gear or bringing the oncoming synchronizer to the sure engaged position (see section 5.3).
The maximum and minimum physical torque limitations of the ICE, BAS and EM are considered when creating the controller output signals. Furthermore, the response delay of powertrain actuators is also taken into account. In particular, for the ICE and the EMs, first order systems are considered ([22, 30]). A rate limit is considered for the clutch transmissible torque variation ([17]). The main parameters employed to model the mentioned response delays are:
rate limit for clutch transmissible torque variation: ±4000 Nm/s;
time constant for ICE: $2.7/\omega_{ICE}(t)$ with $\omega_{ICE}(t)$ being the ICE angular speed in rad/s;
time constant for EM and BAS: 0.0013 s.
The main objectives, control outputs and exit conditions established for each phase are discussed in the following. Furthermore, in appendixes II and III, the exit conditions together with the main controller parameters are presented for both variants of the powertrains.

Phase I: Go-to-slip

The goal of this phase is to reduce the offgoing clutch transmissible torque until slippage starts.
This phase can be considered as a preparation stage before the actual gearshift maneuver starts. It was seen in simulation, for the two powertrain architectures studied, that requesting the torque computed in Eq. (32) before the offgoing clutch starts to slip could result in undesirable driveline oscillations. Hence, in the first phase, the torque request at the transmission input is computed based on the transmission ratio of the offgoing gear as:

$$T_{pr}(t) = ICE_{map}\big(APP(t), \omega_s(t)\tau_{pr}\big) \tag{33}$$

For all the other phases the torque request is computed as explained in section 4.
In the simulations presented in section 8, it is assumed that the powertrain operates in ICE only mode before the gearshift control takes over, i.e., $T_{EM}(t) = 0$ and $T_{ICE,eq}(t) = T_{pr}(t)$.
The clutch transmissible torque is ramped from its maximum value towards zero. The time duration of the transmissible torque ramp (0.1 s) is selected based on the capabilities of the clutch actuators.
For the exit condition for phase I, the clutch is required to slip, i.e., $T_{o,c}(t) \leq T_c(t)$. Note that the torque passing through the clutch is computed with Eq. (1) based on the crankshaft speed measurements.

Phase II: Opening the clutch completely

The main goal is to open the clutch completely while meeting the torque request at the wheels. Hence, the clutch transmissible torque continues to be ramped down as in the previous phase.
The EM connected to the AMT output allows to compensate for the difference between the torque passing through the clutch and the request at the wheels. It is worth mentioning, that the EM torque is kept positive during all the phases of the control logic

For Peer Review

to avoid stressing the mechanical components of the transmission. This is also valid for the DCT powertrain variant.
The torque request to the ICE is computed using a PI controller superimposed to a feedforward term:

$$T_{ICE,eq}(t) = PI\left(\omega_{ICE,ref}(t) - \omega_{ICE}(t)\right) + \left[T_c(t) + J_{ICE,eq}\dot{\omega}_{ICE,ref}(t)\right] \quad (34)$$

The ICE reference speed $\omega_{ICE,ref}(t)$ is computed to keep the clutch slip velocity positive:

$$\omega_{ICE,ref}(t) = \bar{\omega}_s(t)\tau_{pr} + \Delta\omega_{th,p2} \quad (35)$$

In order to avoid wasting energy forcing the crankshaft to follow the speed oscillations of the secondary shaft, the mean value of the transmission output shaft angular speed $\bar{\omega}_s(t)$ (calculated online) is used when creating the ICE speed reference. Moreover, a high enough speed threshold $\Delta\omega_{th,p2}$ (20 rad/s) is selected to force positive slip. When the clutch is slipping, the torque is equal to the transmissible torque and its sign corresponds to that of the slip velocity ([23, 24]). Hence, a linear trend of reduction of the clutch transmissible torque will imply a linear increase of the EM torque request which is preferred to other control signals with higher dynamics. The latter consideration arises from the fact that powertrain actuators are not able to respond immediately to a given command, therefore, torque requests to the EM with lower dynamics are more likely to be fulfilled.
The clutch must be completely open at the end of the second phase.

Phase III: Disengage current gear / Speed synchronization / Engage new gear

The objectives are to disengage the current gear and to use the oncoming synchronizer to force the speed of the primary shaft to match the speed of the secondary shaft with the new gear ratio so that the oncoming gear can be engaged.
Therefore, the first action undertaken is to completely disengage the outgoing synchronizer. Only then, the ingoing synchronizer is commanded to move until its friction elements are in contact, thus allowing to perform the speed synchronization process. Note that, besides supplying for the torque request at the wheels, the EM needs to compensate for the torque that will be transmitted through the friction elements of the synchronizer.
Moreover, the ICE torque is computed as in Eq. (34). The ICE reference speed is ramped from the final value it had on the previous phase towards the speed that the primary shaft would have once the requested gear is engaged ($\omega_s(t)\tau_n$). A high enough angular speed threshold $\Delta\omega_{th,p3}$ (40 rad/s) is considered to pursue positive slip velocity. At the end of the speed ramp, the reference becomes: $\omega_{ICE,ref}(t) = \omega_s(t)\tau_n + \Delta\omega_{th,p3}$.
Phase III ends when the next gear is completely engaged, i.e., when the speeds of primary and secondary shaft are almost the same, thus allowing the ingoing synchronizer to reach the fully engaged position.

Phase IV: Prepare to start closing the clutch

For Peer Review

This phase is added to guarantee that there is positive slip velocity at the time at which the clutch starts to be closed. Hence, the clutch is kept open and the EM is responsible for supplying the torque request at the wheels while the ICE is controlled as in phase II.
The exit condition is that the clutch slip speed must be higher than a certain threshold (30 rad/s).

Phase V: Clutch slip control for engagement

In this phase, the clutch re-engagement is performed. As explained in [11, 15 and 18], a clutch engagement with both slip speed and acceleration equal to zero leads to minimum driveline oscillations. Hence, a parabolic trend is used as a reference for the ICE speed ([11]):

$$\omega_{ICE,ref}(t) = \omega_s(t)\tau_n \frac{\omega_{ICE,p4} - \omega_s(t)\tau_n}{t_{p5}^2}\left(t - t_{p5}\right)^2 \tag{36}$$

where $\omega_{ICE,p4}$ is the ICE speed reference at the end of phase IV. In case the exit conditions are not satisfied at the end of the parabolic fillet, the speed reference is set equal to the speed of the primary shaft. Note that the ICE torque request is computed according to Eq. (34).
In the meantime, the clutch transmissible torque is ramped in open loop towards the current value of the torque request at the transmission input $T_n(t)$. At the end of the torque ramp, the request becomes $T_{o,c}(t) = T_n(t)$.
As in previous phases, the EM supplies the difference between the torque requested at the wheels and the one passing by the clutch.
As it can be inferred from the previous remarks, the clutch slip speed is required to be within a certain small threshold (2 rad/s) before the end of this phase.

Phase VI: Close the clutch completely

In order to conclude the gearshift maneuver, the clutch needs to be completely closed. Therefore, its transmissible torque is ramped towards its maximum value $T_{o,c,max}$.
During this phase, the ICE is commanded to provide the requested torque, i.e., $T_{ICE,eq}(t) = T_n(t)$, while the EM supplies the difference between that same request and the torque actually passing through the clutch.

Gearshift control for HEV powertrains equipped with DCTs: Upshift maneuvers

For the DCT variant of the powertrain architecture of interest, two different control strategies for upshift and downshift maneuvers are presented. The reader is referred to [7–9] and [17] for more information about the gearshift process for both conventional and hybrid DCTs. In this section, the control logic designed to improve gearshift quality during upshifts is addressed.
Similarly to the previous controller, the gearshift process is divided into six consecutive phases (see Figure 6-b):
Phase I: Go-to-slip.

For Peer Review

Phase II: Prepare for torque phase.
Phase III: Torque phase.
Phase IV: Inertia phase - Fast speed matching.
Phase V: Inertia phase - Clutch slip control for engagement.
Phase VI: Close the clutch completely.
The designed controller relies only on speed measurements that are usually available in commercial vehicles:
ICE angular speed;
transmission output shaft angular speed.
The controller output signals are:
torque request to EM;
torque request to ICE;
clutch transmissible torque request.
For this powertrain, the same considerations stated for the AMT variant apply, regarding the use of the output signals and how the response delay of powertrain actuators is accounted for.

Phase I: Go-to-slip

The output signals and exit conditions of this phase are generated similar to what it is explained in section 5.1. The clutch whose transmissible torque is ramped down is the offgoing one. Instead, the oncoming clutch is kept fully open.

Phase II: Prepare for torque phase

The main objective of phase II is to have enough torque available at the DCT input to enforce positive slip on the offgoing clutch in the next phase when power starts being transmitted by the oncoming clutch.
During this phase, the transmissible torque of the offgoing clutch continues to be ramped towards zero as in the previous one while the EM compensates the torque passing through the DCU to meet the request at the wheels.
The torque request to the ICE is computed using a PI superimposed to a feedforward term:

$$T_{ICE,eq}(t) = PI\left(\omega_{ICE,ref}(t) - \omega_{ICE}(t)\right) + \left[T_{c,pr}(t) + T_{c,n}(t) + J_{ICE,eq}\dot{\omega}_{ICE,ref}(t)\right] \quad (37)$$

The ICE reference speed is computed to keep the clutch slip velocity positive: a threshold high enough above the primary shaft speed is chosen (20 rad/s).
The offgoing clutch is required to slip before the end of this phase, i.e., $T_{o,c,pr}(t) \leq T_{c,pr}(t)$. In addition, its transmissible torque must be equal or lower than the minimum between the 70 % of the maximum available torque at the transmission input (ICE + BAS) and the actual torque request. The latter condition is established to ensure that there is enough available torque at the transmission input to guarantee positive slip velocity at the offgoing clutch in the following phase. This can be seen as a saturation of the torque transmitted by the offgoing clutch, i.e.:

For Peer Review

$$T_{o,c,pr} = \frac{min\left(0.7\, T_{in,max}(t)\tau_n, T_n(t)\tau_n\right)}{\tau_{pr}} \tag{38}$$

with

$$T_{in,max}(t) = T_{ICE,max}(t) + T_{BAS,max}(t) \tag{39}$$

where $T_{ICE,max}(t)$ and $T_{BAS,max}(t)$ are the maximum torque available from the ICE and the BAS.

Phase III: Torque phase

The goal is to completely open the offgoing clutch and to start transmitting power through the oncoming clutch while meeting the torque request at the wheels.
The control of the slip velocity at the offgoing clutch is the main challenge. As explained in phase II, to ensure there is enough available torque at the transmission input, the transmissible torque is saturated. Instead of controlling both clutches to transmit the torque necessary to supply for the request $T_n(t)$, the minimum value between this quantity and the 70 % of the maximum available torque at the DCT input computed with Eq. (39) is considered. In addition, a PI is used to introduce a correction to the transmissible torque request aiming at achieving the desired slipping rate. Based on the previous considerations, it holds:

$$T_{o,c,pr}(t) = \frac{\left(min\left(0.7\, T_{in,max}(t), T_n(t)\right) - T_{c,n}(t)\right)\tau_n}{\tau_p} + PI\left(\omega_{cs,ref}(t) - \omega_{cs}(t)\right) \tag{40}$$

Note that the angular slip speed reference is ramped from the initial value at the beginning of this phase towards the desired target (20 rad/s) to avoid discontinuities in the transmissible torque.
The transmissible torque of the oncoming clutch is ramped towards the desired value at the transmission input, i.e., $min\left(0.7\, T_{in,max}(t), T_n(t)\right)$, in open loop.
Finally, the EM and the ICE are controlled as in the previous phase.
The exit conditions require the offgoing clutch to be open.

Phase IV: Inertia phase - Fast speed matching

The goal is to decrease as fast as possible the speed of the ICE towards the speed of the oncoming clutch. In the subsequent control stage, in order to perform a smooth clutch engagement, the slip speed is controlled more carefully.
During phase IV, the ICE torque is computed as in Eq. (37). The reference speed is computed to match a certain threshold $\Delta\omega_{th,p4}$ (40 rad/s) above the angular speed of the oncoming clutch. A ramp is imposed in order give a continuous reference to the ICE. After the speed ramp is undertaken, the reference becomes: $\omega_{ICE,ref}(t) = \omega_s(t)\tau_n + \Delta\omega_{th,p4}$.
Moreover, the transmissible torque of the oncoming clutch is ramped towards its target value in open loop. After the end of the transmissible torque ramp, the request is: $T_{o,c,n}(t) = T_n(t)$. Note that the EM is used to compensate the torque passing through this clutch to meet the power request at the wheels.

For Peer Review

This phase ends once the slip speed on the oncoming is within a certain threshold (45 rad/s).

Phase V: Inertia phase - Clutch slip control for engagement

The goal is now to achieve a very precise control of the slip velocity at the oncoming clutch in order to have smooth clutch engagement. As previously stated, this is achieved when the slip speed and acceleration at clutch lock-up are close to zero.
As for the AMT variant of the powertrain, a parabolic fillet is imposed as a reference to the ICE speed to force the angular slip speed and acceleration to be zero at the time the clutch is engaged (see section 5.5).
In addition, the EM compensates the torque passing through the oncoming clutch (controlled as in the previous phase) to meet the request at the wheels.
The same exit conditions established for phase V of the AMT control logic are considered (see section 5.5).

Phase VI: Close the clutch completely

The output signals and exit conditions are designed similarly to section 5.6 for the AMT variant.

Gearshift control for HEV powertrains equipped with DCTs: Downshift maneuvers

The control logic designed to improve gearshift quality during downshifts is divided into four consecutive phases (see Figure 9-b):
Phase I: Go-to-slip.
Phase II: Inertia phase - Fast speed matching.
Phase III: Torque phase - Clutch slip control for engagement.
Phase IV: Close the clutch completely.
The required inputs and outputs correspond to those of the algorithm developed for upshift maneuvers.

Phase I: Go-to-slip

This phase is undertaken as explained for the upshifts (see section 6.1).

Phase II: Inertia phase - Fast speed matching

The goal of this phase is to increase as fast as possible the speed of the ICE towards a certain threshold (40 rad/s) above the speed of the oncoming clutch. The torque request to the ICE is computed as described for the upshift maneuvers during phase IV (see section 6.4). The duration of the speed ramp (0.3 s) is selected in order to provide a suitable reference for the crankshaft speed according to the capabilities of the powertrain actuators.

For Peer Review

The offgoing clutch is controlled to minimize clutch slip losses. Hence, its transmissible torque is ramped to compensate the difference between the maximum torque available from the EM and the actual torque request. Note that, since the latter component is used as a torque fill device, the clutch will be fully open (thus eliminating slip losses), if the EM alone can deliver the whole requested torque. Once the transmissible torque ramp is undertaken, the request to the offgoing clutch becomes:

$$T_{o,c,pr}(t) = \frac{T_n(t)\tau_n - T_{EM,max}(t)\tau_{EM}}{\tau_{pr}} \tag{41}$$

where $T_{EM,max}(t)$ is the maximum available torque from the EM.
In order to validate the transition to the next phase, the ongoing clutch slip velocity must be equal or higher than a certain threshold (40 rad/s).

Phase III: Torque phase - Clutch slip control for engagement

In order to realize a very precise control of the slip velocity on the oncoming clutch, the ICE torque request is computed as explained for phase V of the upshift control strategy (see section 6.5). In addition, for the clutch slip control to exploit the maximum of the DCT capabilities, the oncoming clutch is also controlled to help reducing of the driveline oscillations at the time of engagement. Therefore, its transmissible torque is ramped towards the value requested by the driver while a PI is used to introduce a correction aiming at enforcing the desired slipping rate:

$$T_{o,c,n}(t) = \frac{T_n(t)}{t_{p3}}t + PI\left(\omega_{ICE,ref}(t) - \omega_{ICE}(t)\right) \tag{42}$$

where t_{p3} is the duration of the transmissible torque ramp (0.1 s). After t_{p3} the transmissible torque is:

$$T_{o,c,n}(t) = T_n(t) + PI\left(\omega_{ICE,ref}(t) - \omega_{ICE}(t)\right) \tag{43}$$

The speed reference seen in Eq. (42) and Eq. (43) is the same used to generate the ICE torque request (see section 6.5).
The offgoing clutch, if not already open, is required to compensate the difference between the torque request and the torque passing through the oncoming clutch. The maximum value that the transmissible torque can take is the one at the end of the previous phase.
Finally, the EM continues to be used as a torque fill device.
The offgoing clutch must be completely disengaged at the end of this phase. In addition, the slip velocity in the oncoming clutch is required to be within a small threshold (2 rad/s).

Phase IV: Close the clutch completely

The last phase of the algorithm described in this section is identical to the last phase of the upshift control strategy (see section 6.6).

Simulation results

For Peer Review

Simulation results are presented and analyzed to illustrate the effectiveness of the gearshift control strategies designed for the two variants of the powertrain. In addition, the results are also used to establish the benefits and limitations of the two transmission systems.
For each of the gearshift maneuvers, the powertrain model is initialized starting at a predefined speed from which the vehicle is driven using only the ICE to satisfy the torque request at the wheels. In all the simulations performed, the gearshift process starts after 2.5 s.
Moreover, the transmission ratios of the DCT and the AMT are set to be the same. In this way, the differences seen in the vehicle performance are likely to be related mostly to the functioning principle of each transmission technology.

Upshift maneuver: 1st to 2nd at 100% APP

Simulation results for a 1st to 2nd upshift performed at 100 % APP are presented for both the H-DCT and the H-AMT.
The upper plot of Figure 6 shows the speeds of the main driveline components, including the ICE reference speed which is set to zero when the crankshaft speed is not being controlled. Instead, the lower plot shows the torque request to the ICE and the EM together with the clutches and synchronizers transmissible torque. The actual torque passing through the clutches is also presented.
Note that for the H-AMT, phase IV is skipped since the clutch slip speed at the end of phase III is above the specified threshold used as an exit condition for phase IV (see section 5.4).
Due to the limited amount of braking torque that can be provided by the ICE and the BAS, for the H-AMT, during phases III and V the ICE speed does not properly follows its reference. This limitation does not lead to undesired vibrations thanks to the way in which the EM is controlled. Instead, the H-DCT is able to properly follow the ICE speed reference.
"[insert Figure 6-a.]"
a) H-AMT
"[insert Figure 6-b.]"
b) H-DCT

Figure 6. Speed and torque: 1st to 2nd at 100 % APP: (a) AMT; (b) DCT.

"[insert Figure 7.]"

Figure 7. Speed and torque (H-AMT): 4th to 5th at 100% APP.

Figure 7 shows the results of a 4th to 5th upshift performed at 100% APP by the H-AMT in which the powertrain is able to follow the imposed reference speed considerably better. This translates into an almost linear decrease during phase II (and increase in phase V) of the torque passing by the clutch; consequently, the EM torque shows a very smooth change rate, which is more likely to be successfully provided by the motor.
In a conventional (non-hybrid) AMT, speed oscillations in the primary shaft arise when the torque starts again passing through the clutch, after the torque gap occurring during the synchronization phase. In the H-AMT, thanks to the action of the EM, the secondary shaft is never unloaded. This leads to two advantages: first, it reduces the input shaft

For Peer Review

vibrations at the beginning of phase V. Secondly, it enables the possibility of performing the clutch slip control while the transmissible torque is being ramped-up, making the gearshift process faster.

In addition, the energy required for torque gap filling from the EM by the H-AMT is considerably larger than that of the H-DCT (see Table 2). Note that, given the architecture of the AMT, during phase III, the EM has to supply the entire power request at the wheels.

"[insert Figure 8-a.]"

a) H-AMT

"[insert Figure 8-b.]"

b) H-DCT

Figure 8. Acceleration and Jerk: 1st to 2nd at 100 % APP: (a) AMT; (b) DCT.

In Figure 8, the longitudinal acceleration and jerk during the gearshift maneuver are presented. A very smooth clutch engagement is achieved for both powertrain architectures as indicated by the low jerk value at the end of phase V. As expected, based on the fact that the H-DCT is able to follow better the ICE speed reference, the maximum (absolute) jerk value for the H-AMT in phase VI is higher than that of the other powertrain (1.35 m/s^3 vs. 0.55 m/s^3). Furthermore, Figure 8 shows that the main jerk peak is due to the increase in the torque delivered to the wheels to satisfy the request expressed by the driver. However, using a time constant of 0.05 s for the torque request transition, the maximum jerk value is always under 10 m/s^3. In [31], the experiments conducted shown than a value greater than 10 m/s^3 is perceived by the passengers as uncomfortable. Table 2 presents the value of the gearshift quality metrics described in section 3. In terms of the vehicle performance and shift comfort, it can be seen that the results obtained for both powertrains are similar. Note that the torque request at the wheels is satisfied slightly better by the H-DCT as quantified by its mean torque error. Instead, by looking at the energy consumption indicators, it can be noted that the H-DCT presents a significantly higher energy loss due to clutch slip (two clutches are slipping during the gearshift instead of one). On the other hand, as explained when discussing Figure 6, the energy requested from the EM is larger for the H-AMT. The global energy balance made considering these two indicators shows that the H-DCT is more energy efficient during upshifts.

Table 2. Gearshift quality criteria: 1st to 2nd at 100 % APP.

Gearshift quality criteria	Parameter	H-AMT	H-DCT
Performance	t_{gs} [s]	0.696	0.545
	$\bar{a}$ [m/s2]	2.942	2.933
	$\bar{T}_{w,err}$ [%]	1.680	0.742
Shift	$Jerk_{RMS}$	2.482	3.290

For Peer Review

comfort	[m/s3]		
	$Jerk_{max/\min}$ [m/s3]	13.596	14.028
Shift efficiency	$E_{c,dis}$ [kJ]	0.825	10.624
Torque fill energy consumption	E_{EM} [kJ]	47.702	9.839

8.2 Downshift maneuver: 4th to 3rd at 100% APP

Simulation results for a 4th to 3rd downshift at 100% APP are presented for both H-DCT and H-AMT.

Table 3. Gearshift quality criteria: 4th to 3rd at 100% APP.

Gearshift quality criteria	**Parameter**	**H-AMT**	**H-DCT**
Performance	t_{gs} [s]	0.448	0.438
	$\bar{a}$ [m/s2]	1.648	1.641
	$\bar{T}_{w,err}$ [%]	0.946	0.803
Shift comfort	$Jerk_{RMS}$ [m/s3]	3.166	3.238
	$Jerk_{max/\min}$ [m/s3]	10.375	11.165
Shift efficiency	$E_{c,dis}$ [kJ]	0.272	0.352
Torque fill energy consumption	E_{EM} [kJ]	24.352	22.915

Differently form the upshift maneuver, during downshifts, the ICE reference speed is followed well by both powertrains, as shown in Figure 9. Furthermore, it is worth noting that, to minimize clutch slip energy losses for the H-DCT, the EM works as a torque fill device similarly to the H-AMT (see section 7.2).

For Peer Review

"[insert Figure 9-a.]"
a) H-AMT
"[insert Figure 9-b.]"
b) H-DCT

Figure 9. Speed and torque: 4th to 3rd at 100% APP: (a) AMT; (b) DCT.

Figure 10 shows that the torque request at the wheels is matched well by both powertrain variants. This is also expressed by the low mean errors reported in Table 3. Moreover, the effect of the actuation delay of the EM can be appreciated at the times in which the offgoing clutch is being opened or the oncoming one is being engaged. In those instances, the EM is not able to compensate the torque passing through the transmission input in order to meet the exact request at the wheels.
Similarly to upshifts, Figure 11 shows that clutch engagement is smooth.
Table 3 presents the values of the gearshift quality parameters for both powertrains. In terms of vehicle performance and shift comfort, the value of the selected indicators is almost the same for H-AMT and H-DCT. Moreover, since the EM is used in a similar manner by both systems, the clutch slip losses and torque fill energy are also comparable, with the H-DCT performing slightly better.
"[insert Figure 10-a.]"
a) H-AMT
"[insert Figure 10-b.]"
b) H-DCT

Figure 10. Torque at the wheels: 4th to 3rd at 100% APP: (a) AMT; (b) DCT.

"[insert Figure 11-a.]"
a) H-AMT
"[insert Figure 11-b.]"
b) H-DCT

Figure 11. Acceleration and Jerk: 4th to 3rd at 100% APP: (a) AMT; (b) DCT.

Conclusions

In this paper, in order to assess gearshift quality and its impact on drivability, nonlinear dynamic models of a series-parallel HEV are developed. Two variants of this powertrain are studied: H-AMT and H-DCT. In both architectures, an EM is connected to the driveshaft through a mechanical coupler enabling full or partial compensation of the torque gap during gearshifts. Thanks to the model features, the first torsional mode of the driveline can be correctly estimated and an assessment of the vehicle drivability can be exploited.
Gearshift control strategies for both powertrains are developed: the proposed algorithms are simple to implement and tune since they are based on PI controllers.
The results obtained for both HEV architectures are promising in terms of vehicle dynamic performance. One fundamental advantage is that for the H-AMT it was possible to significantly reduce the torque gap during gearshifts, while keeping the mechanical complexity of the system lower with respect to H-DCT. The simulations allow to assess that the main differences in performance take place during upshift maneuvers where the

For Peer Review

energy requested from the EM is larger for the H-AMT. Hence, during this type of gearshifts, the H-DCT is shown to be more energy efficient. Instead, during downshifts, in order to minimize clutch slip losses for the H-DCT, the EM works as a torque fill device, similarly to the H-AMT; thus the energy consumption indicators of the powertrains are comparable.

Further work should focus on different topics: experimental validation of the developed models, onboard implementation of the proposed controllers, assessment of the controller robustness against disturbance and of the interaction of the proposed algorithms with energy management strategies.

Funding statement

This research received no specific grant from any funding agency in the public, commercial, or not-for-profit sectors.

Declaration of conflicting interests

The authors declare that there is no conflict of interest.

References

[1] S. Onori, L. Serrao, and G. Rizzoni, *Hybrid Electric Vehicles: Energy Management Strategies*, 1st ed. Springer-Verlag London, 2016.

[2] M. Awadallah, P. Tawadros, P. Walker, and N. Zhang, "Dynamic modelling and simulation of a manual transmission based mild hybrid vehicle," *Mech. Mach. Theory*, vol. 112, pp. 218–239, 2017.

[3] E. Galvagno, M. Velardocchia, and A. Vigliani, "Dynamic and kinematic model of a dual clutch transmission," *Mech. Mach. Theory*, vol. 46, no. 6, pp. 794–805, 2011.

[4] E. Galvagno, G. R. Guercioni, and A. Vigliani, "Sensitivity Analysis of the Design Parameters of a Dual-Clutch Transmission Focused on NVH Performance," *SAE Tech. Pap. 2016-01-1127*, 2016.

[5] J. Kim *et al.*, "Simulation of the shift force for a manual transmission," *Proc. Inst. Mech. Eng. Part D J. Automob. Eng.*, vol. 217, no. 7, pp. 573–581, 2003.

[6] B. Gao, Y. Lei, A. Ge, H. Chen, and K. Sanada, "Observer-based clutch disengagement control during gear shift process of automated manual transmission," *Veh. Syst. Dyn.*, vol. 49, no. 5, pp. 685–701, 2011.

[7] K. van Berkel, T. Hofman, A. Serrarens, and M. Steinbuch, "Fast and smooth clutch engagement control for dual-clutch transmissions," *Control Eng. Pract.*, vol. 22, pp. 57–68, 2014.

[8] M. Goetz, M. C. Levesley, and D. A. Crolla, "Dynamics and control of gearshifts on twin-clutch transmissions," *Proc. Inst. Mech. Eng. Part D J. Automob. Eng.*, vol. 219, no. 8, pp. 951–963, 2005.

[9] Y. Liu, D. Qin, H. Jiang, and Y. Zhang, "Shift control strategy and experimental validation for dry dual clutch transmissions," *Mech. Mach. Theory*, vol. 75, pp. 41–53, 2014.

For Peer Review

[10] G. Li and D. Görges, "Optimal control of the gear shifting process for shift smoothness in dual-clutch transmissions," *Mech. Syst. Signal Process.*, vol. 103, pp. 23–38, 2018.

[11] F. Amisano, E. Galvagno, M. Velardocchia, and A. Vigliani, "Automated manual transmission with a torque gap filler Part 2: Control and experimental validation," *Proc. Inst. Mech. Eng. Part D J. Automob. Eng.*, vol. 228, no. 14, pp. 1700–1717, 2014.

[12] L. Glielmo, L. Iannelli, V. Vacca, and F. Vasca, "Gearshift Control for Automated Manual Transmissions," *IEEE/ASME Trans. Mechatronics*, vol. 11, no. 1, pp. 17–26, 2006.

[13] X.-Y. Song, Z.-X. Sun, X.-J. Yang, and G.-M. Zhu, "Modelling, control, and hardware-in-the-loop simulation of an automated manual transmission," *Proc. Inst. Mech. Eng. Part D J. Automob. Eng.*, vol. 224, no. 2, pp. 143–160, 2010.

[14] Z. Lei, D. Sun, Y. Liu, D. Qin, and Y. Zhang, "Analysis and coordinated control of mode transition and shifting for a full hybrid electric vehicle based on dual clutch transmissions," *Mech. Mach. Theory*, vol. 114, pp. 125–140, 2017.

[15] A. M. Gavgani, A. Sorniotti, J. Doherty, and C. Cavallino, "Optimal gearshift control for a novel hybrid electric drivetrain," *Mech. Mach. Theory*, vol. 105, pp. 352–368, 2016.

[16] A. Mehdizadeh Gavgani, T. Bingham, A. Sorniotti, J. Doherty, C. Cavallino, and M. Fracchia, "A Parallel Hybrid Electric Drivetrain Layout with Torque-Fill Capability," *SAE Int. J. Passeng. Cars - Mech. Syst.*, vol. 8, no. 2, pp. 767–778, 2015.

[17] V. Ranogajec and J. Deur, "Bond graph analysis and optimal control of the hybrid dual clutch transmission shift process," *Proc. Inst. Mech. Eng. Part K J. Multi-body Dyn.*, vol. 231, no. 3, pp. 480–492, 2017.

[18] F. Garofalo, L. Glielmo, L. Iannelli, and F. Vasca, "Smooth engagement for automotive dry clutch," in *Proceedings of the 40th IEEE Conference on Decision and Control*, 2001, vol. 1, pp. 529–534.

[19] Z.-G. Zhao, H.-J. Chen, Y.-Y. Yang, and L. He, "Torque coordinating robust control of shifting process for dry dual clutch transmission equipped in a hybrid car," *Veh. Syst. Dyn. Int. J. Veh. Mech. Mobil.*, vol. 53, no. 9, pp. 1269–1295, 2015.

[20] J. Deur, J. Asgari, and D. Hrovat, "Modeling and Analysis of Automatic Transmission Engagement Dynamics-Nonlinear Case Including Validation," *J. Dyn. Syst. Meas. Control*, vol. 128, no. 2, pp. 251–262, 2005.

[21] M. Kulkarni, T. Shim, and Y. Zhang, "Shift dynamics and control of dual-clutch transmissions," *Mech. Mach. Theory*, vol. 42, no. 2, pp. 168–182, 2007.

[22] E. Galvagno, D. Morina, A. Sorniotti, and M. Velardocchia, "Drivability analysis of through-the-road-parallel hybrid vehicles," *Meccanica*, vol. 48, no. 2, pp. 351–366, 2013.

[23] E. Pennestrì, V. Rossi, P. Salvini, and P. P. Valentini, "Review and comparison of dry friction force models," *Nonlinear Dyn.*, vol. 83, no. 4, pp. 1785–1801, 2016.

[24] T. Piatkowski, "Dahl and LuGre dynamic friction models - The analysis of selected properties," *Mech. Mach. Theory*, vol. 73, pp. 91–100, 2014.

[25] Hans B. Pacejka, *Tyre and Vehicle Dynamics*, 2nd ed. Butterworth-Heinemann,

For Peer Review

2006.
[26] B. wook Jeon and S.-H. Kim, "Measurement and Modeling of Perceived Gear Shift Quality for Automatic Transmission Vehicles," *SAE Int. J. Passeng. Cars - Mech. Syst.*, vol. 7, no. 1, pp. 423–433, 2014.
[27] T. D'Anna, K. Govindswamy, F. Wolter, and P. Janssen, "Aspects of Shift Quality With Emphasis on Powertrain Integration and Vehicle Sensitivity," *SAE Tech. Pap. 2005-01-2303*, 2005.
[28] J. M. W. Brownjohn and X. Zheng, "Discussion of human resonant frequency," in *International Conference on Experimental Mechanics*, 2001, vol. 4317, pp. 469–474.
[29] K. M. Bovee, "Optimal Control of Electrified Powertrains with the Use of Drive Quality Criteria," Ohio State University, 2015.
[30] K. Koprubasi, G. Rizzoni, E. Galvagno, and M. Velardocchia, "Development and experimental validation of a low-frequency dynamic model for a Hybrid Electric Vehicle," *Int. J. Powertrains*, vol. 1, no. 3, pp. 304–333, 2012.
[31] Q. Huang and H. Wang, "Fundamental Study of Jerk: Evaluation of Shift Quality and Ride Comfort," *SAE Tech. Pap. 2004-01-2065*, 2004.

Appendix I

Abbreviations

AMT	Automated Manual Transmission
APP	Accelerator Pedal Position
BAS	Belt Alternator Starter
DCT	Dual-Clutch Transmission
DCU	Dual-Clutch Unit
DOF	Degree Of Freedom
ECU	Engine Control Unit
EM	Electric Machine
H-AMT	Hybrid Automated Manual Transmission
H-DCT	Hybrid Dual-Clutch Transmission
HEV	Hybrid Electric Vehicle
ICE	Internal Combustion Engine
MT	Manual Transmission
PI	Proportional-Integral controller
PTU	Power Transfer Unit
RMS	Root Mean Square
SMF	Single Mass Flywheel
TPBVP	Two-Point Boundary-Value Problem

Notation

a	Vehicle longitudinal acceleration
A	Area
APP	APP

For Peer Review

c	Generic coefficient
E	Energy
F	Force
ICE	ICE
J	Rotational inertia
$Jerk$	Jerk
k	Torsional stiffness
M	Vehicle mass
r	Radius
t	Time
T	Torque
v	Vehicle longitudinal speed
α	Road grade angle
$\Delta\omega$	Angular speed difference
θ	Angular position
ρ	Density
τ	Transmission ratio
ω	Angular speed

Subscripts

0	Initial condition
1	First element
2	Second element
aer	Aerodynamic resistance
BAS	BAS
c	Clutch
cd	Clutch disc
cm	Clutch mechanism
cs	Clutch slip
d	Final drive
db	Final drive bearing
dis	Dissipative element
dr	Driven element
Dr	Driving element
eq	Equivalent element
err	Error
ex	Exit condition
EM	EM
f	Final element
g	Road grade
gs	Gearshift
GB	Gearbox
hs	Half-shaft
in	Input
ICE	ICE

For Peer Review

map	Map
max	Maximum value
max/min	Peak-to-peak value
min	Minimum value
n	New element
o	Clutch transmissible torque
p	Primary shaft
pb	Primary shaft bearing
pbr	Primary shaft relative bearing
pj	J^{th} phase
pr	Previous element
PTU	PTU
ref	Reference
rq	Required element
rr	Rolling resistance
RMS	RMS
s	Secondary shaft
sb	Secondary shaft bearing
syn	Synchronizer
SMF	SMF
td	Torsional damper
tdh	Torsional damper hysteretic element
tds	Torsional damper restoring element
th	Threshold
tot	Total value
v	Vehicle
w	Wheel
x	Longitudinal direction
z	Vertical direction

Appendix II

The main control parameters are presented below.

H-AMT

Table 4. Controller parameters: H-AMT.

Phase	Parameter	Value
I	Transmissible torque ramp duration	0.1 s
II	Transmissible torque ramp duration	0.1 s

For Peer Review

	ICE speed reference threshold	20 rad/s
III	ICE speed reference threshold	40 rad/s
	ICE speed reference ramp duration	0.15 s
IV	ICE speed reference threshold	40 rad/s
V	Transmissible torque ramp duration	0.1 s
	ICE speed reference parabolic fillet duration	0.1 s
VI	Transmissible torque ramp duration	0.05 s

H-DCT: upshift maneuvers

Table 5. Controller parameters: H-DCT (upshifts).

Phase	Parameter	Value
I	Offgoing clutch transmissible torque ramp duration	0.1 s
II	Offgoing clutch transmissible torque ramp duration	0.1 s
	ICE speed reference threshold	20 rad/s
III	Offgoing clutch slip speed target	20 rad/s
	Offgoing clutch slip speed reference ramp duration	0.1 s
	Oncoming clutch transmissible torque ramp duration	0.1 s

For Peer Review

	ICE speed reference threshold	20 rad/s
IV	Oncoming clutch transmissible torque ramp duration	0.1 s
	ICE speed reference threshold	40 rad/s
	ICE speed reference ramp duration	0.25 s
V	Oncoming clutch transmissible torque ramp duration	0.1 s
	ICE speed reference parabolic fillet duration	0.1 s
VI	Oncoming clutch transmissible torque ramp duration	0.05 s

H-DCT: downshift maneuvers

Table 6. Controller parameters: H-DCT (downshifts).

Phase	Parameter	Value
I	Offgoing clutch transmissible torque ramp duration	0.1 s
II	Offgoing clutch transmissible torque ramp duration	0.1 s
	ICE speed reference threshold	40 rad/s
	ICE speed reference ramp duration	0.3 s
III	Oncoming clutch transmissible torque ramp duration	0.1 s
	ICE speed reference parabolic fillet duration	0.1 s

For Peer Review

IV	Oncoming clutch transmissible torque ramp duration	0.05 s

Appendix III

Exit conditions for each of the three control logics developed are presented below.

H-AMT

Table 7. Exit conditions: H-AMT.

Phase	Exit condition
I	Clutch slips: $T_{o,c}(t) \leq T_c(t)$
II	Clutch is open: $T_{o,c}(t) = 0\ Nm$
III	Speeds of primary and secondary shaft are within $\Delta\omega_{ex,p3}$ (0.5 rad/s): $\lvert\omega_p(t) - \omega_s(t)\tau_n\rvert \leq \Delta\omega_{ex,p3}$
	Synchronizer reaches the fully engaged position
IV	Clutch slip speed is higher than $\Delta\omega_{ex,p4}$ (30 rad/s): $\lvert\omega_{ICE}(t) - \omega_s(t)\tau_n\rvert \geq \Delta\omega_{ex,p4}$
V	Clutch slip speed is within $\Delta\omega_{ex,p5}$ (2 rad/s): $\lvert\omega_{ICE}(t) - \omega_s(t)\tau_n\rvert \leq \Delta\omega_{ex,p5}$
VI	Clutch is fully closed: $T_{o,c}(t) = T_{o,c,max}$

H-DCT: upshift maneuvers

Table 8. Exit conditions: H-DCT (upshifts).

Phase	Exit condition
I	Offgoing clutch slips: $T_{o,c,pr}(t) \leq T_{c,pr}(t)$
II	Offgoing clutch slips: $T_{o,c,pr}(t) \leq T_{c,pr}(t)$

For Peer Review

	Offgoing clutch transmissible torque is equal or lower than the minimum between the 70 % of the maximum available torque at the transmission input and the actual torque request: $T_{o,c,pr} \leq \frac{min\left(0.7\, T_{in,max}(t)\tau_n, T_n(t)\tau_n\right)}{\tau_{pr}}$
III	Offgoing clutch is open: $T_{o,c,pr}(t) = 0$
IV	Oncoming clutch slip velocity is equal or lower than $\Delta\omega_{ex,p4}$ (45 rad/s): $\omega_{ICE}(t) - \omega_s(t)\tau_n \leq \Delta\omega_{ex,p4}$
V	Oncoming clutch slip velocity is within $\Delta\omega_{ex,p5}$ (2 rad/s): $\lvert\omega_{ICE}(t) - \omega_s(t)\tau_n\rvert \leq \Delta\omega_{ex,p5}$
VI	Oncoming clutch is fully closed: $T_{o,c,n}(t) = T_{o,c,max}$

H-DCT: downshift maneuvers

Table 9. Exit conditions: H-DCT (downshifts).

Phase	Exit condition
I	Offgoing clutch slips: $T_{o,c,pr}(t) \leq T_{c,pr}(t)$
II	Oncoming clutch slip velocity is equal or higher than $\Delta\omega_{ex,p2}$ (40 rad/s): $\omega_{ICE}(t) - \omega_s(t)\tau_n \geq \Delta\omega_{ex,p2}$
III	Oncoming clutch slip velocity is within $\Delta\omega_{ex,p3}$ (2 rad/s): $\lvert\omega_{ICE}(t) - \omega_s(t)\tau_n\rvert \leq \Delta\omega_{ex,p3}$
	Offgoing clutch is open: $T_{o,c,pr}(t) = 0$
IV	Oncoming clutch is fully closed:

For Peer Review

$$T_{o,c,n}(t) = T_{o,c,max}$$

For Peer Review

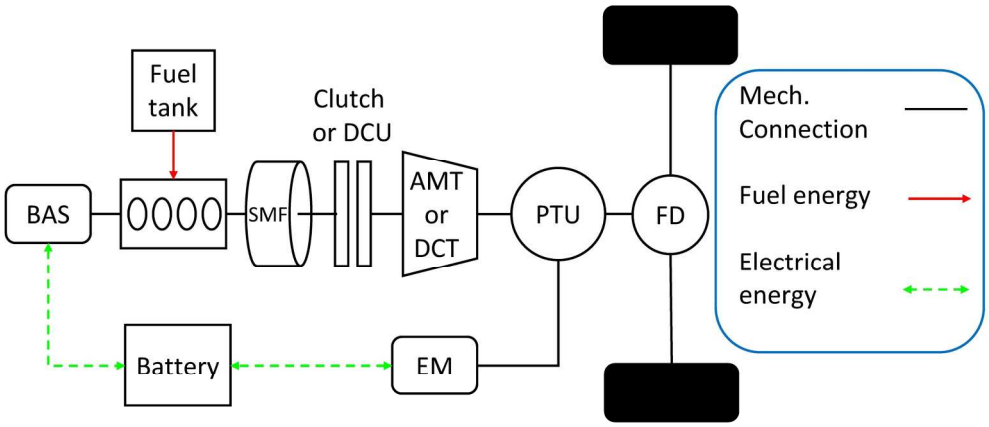

Figure 1. Powertrain layout

190x142mm (300 x 300 DPI)

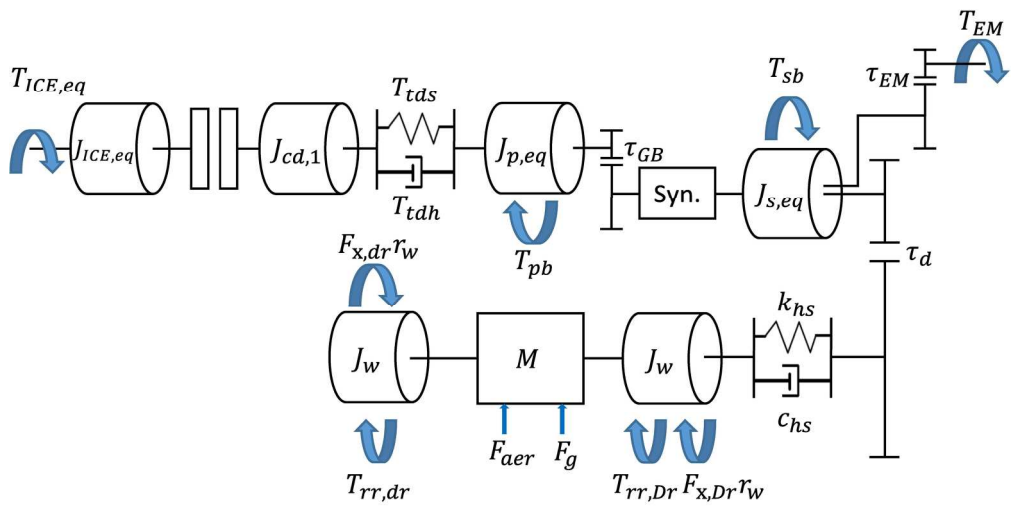

Figure 2. Powertrain model: AMT.

190x142mm (300 x 300 DPI)

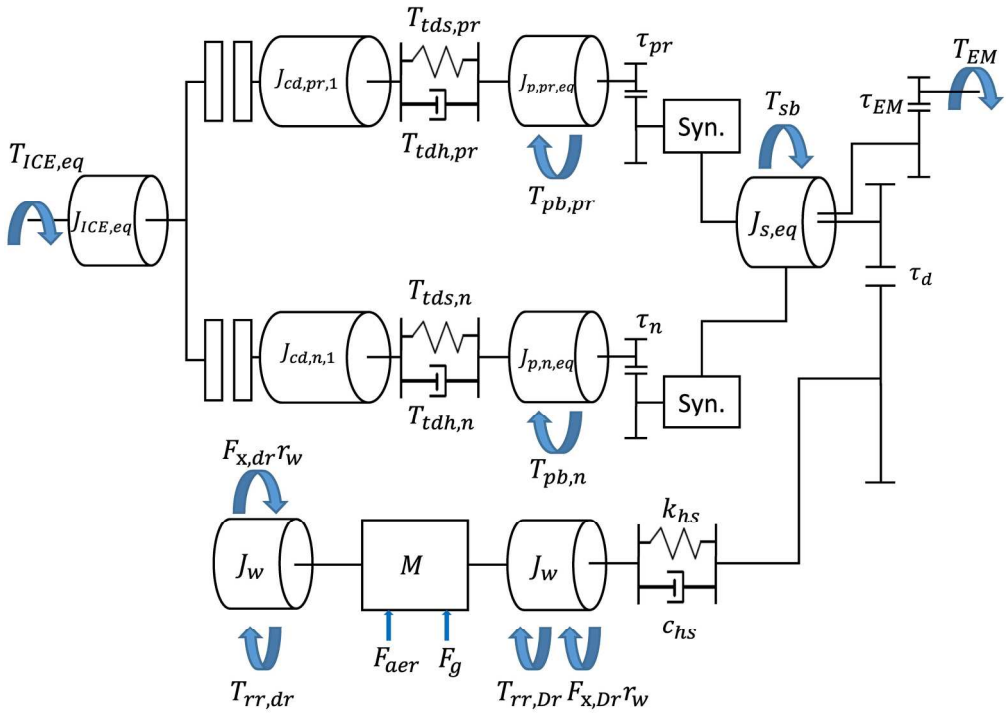

Figure 3. Powertrain model: DCT

190x142mm (300 x 300 DPI)

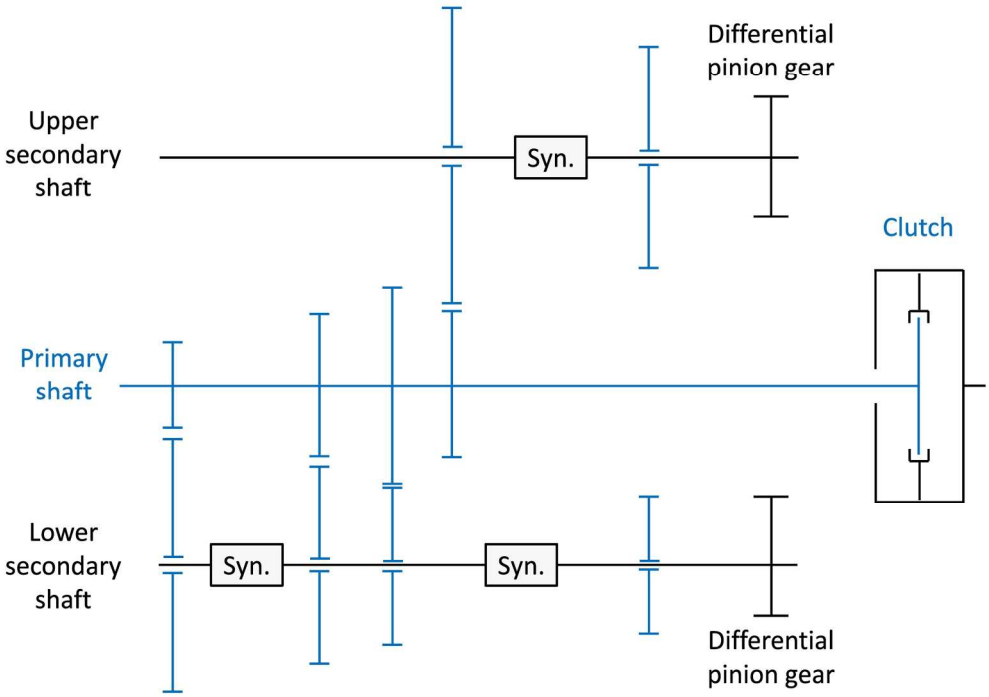

Figure 4. AMT schematic layout

190x142mm (300 x 300 DPI)

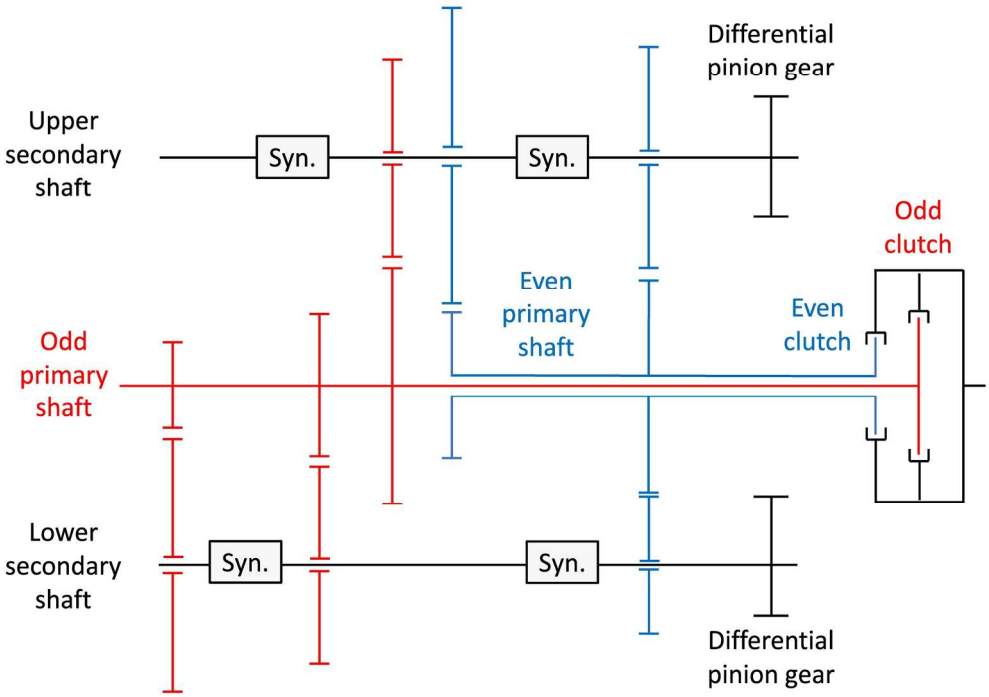

Figure 5. DCT schematic layout

190x142mm (300 x 300 DPI)

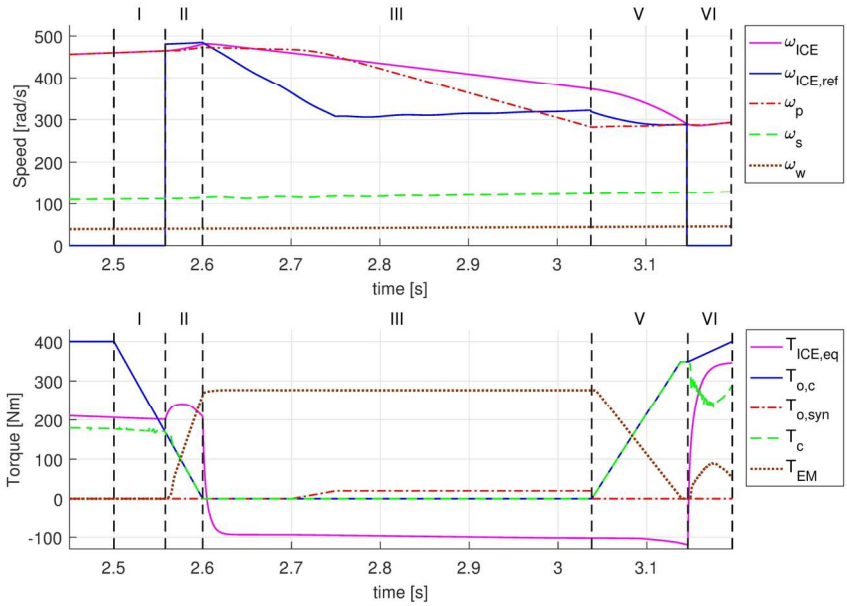

Figure 6. Speed and torque: 1st to 2nd at 100 % APP: (a) AMT; (b) DCT

158x102mm (300 x 300 DPI)

Review

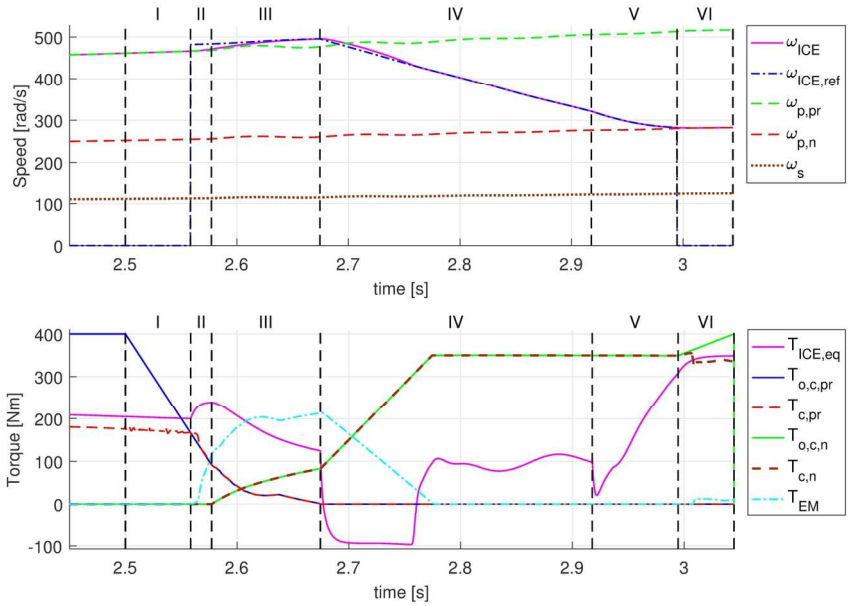

Figure 6. Speed and torque: 1st to 2nd at 100 % APP: (a) AMT; (b) DCT

158x101mm (300 x 300 DPI)

Review

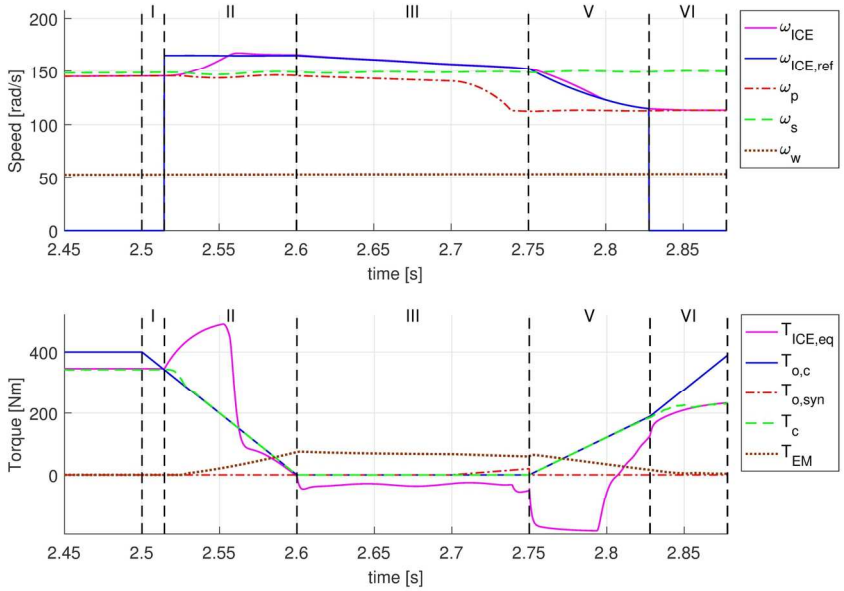

Figure 7. Speed and torque (H-AMT): 4th to 5th at 100% APP

158x102mm (300 x 300 DPI)

Review

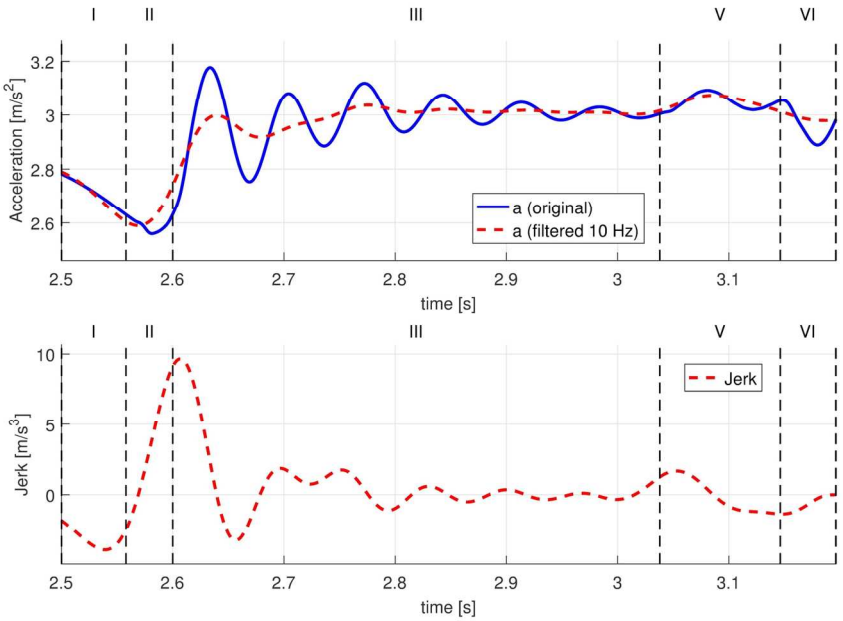

Figure 8. Acceleration and Jerk: 1st to 2nd at 100 % APP: (a) AMT; (b) DCT

158x102mm (300 x 300 DPI)

Review

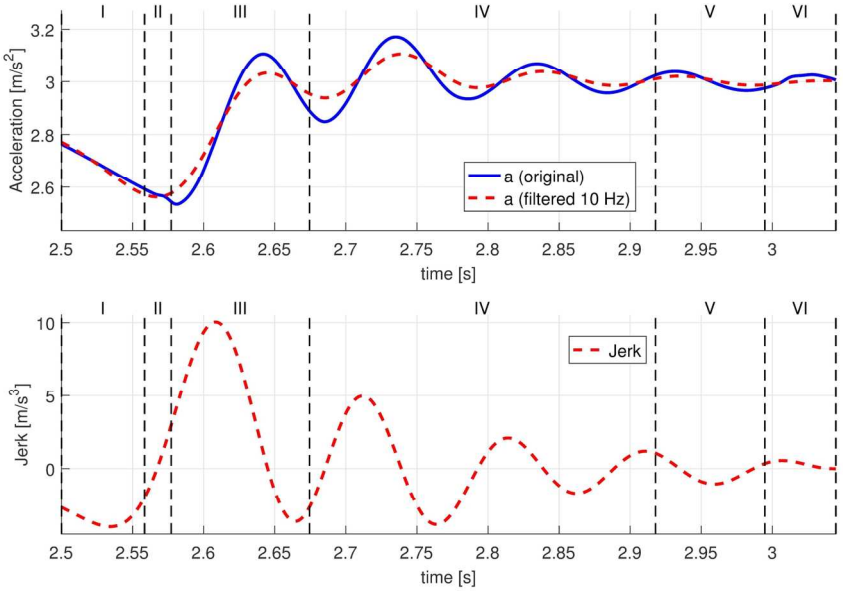

Figure 8. Acceleration and Jerk: 1st to 2nd at 100 % APP: (a) AMT; (b) DCT

158x102mm (300 x 300 DPI)

Review

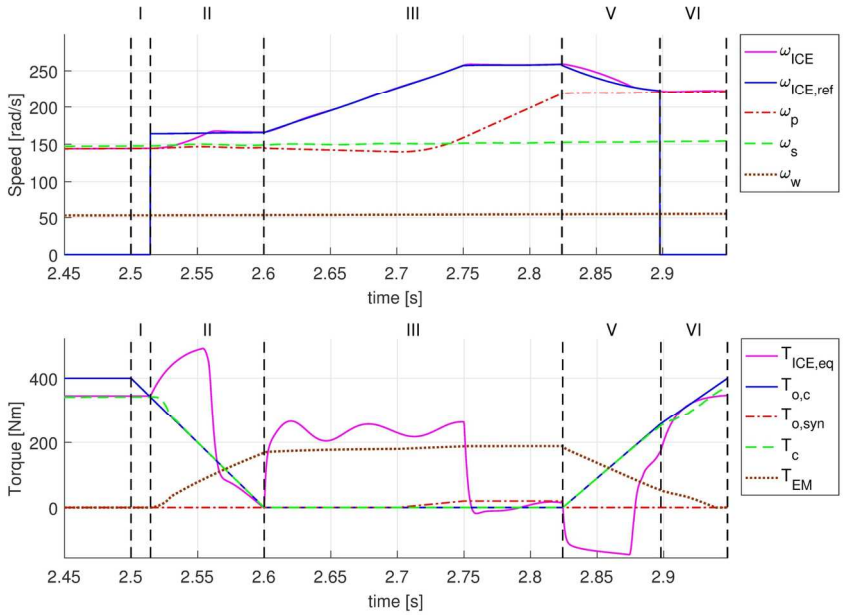

Figure 9. Speed and torque: 4th to 3rd at 100% APP: (a) AMT; (b) DCT

158x102mm (300 x 300 DPI)

Review

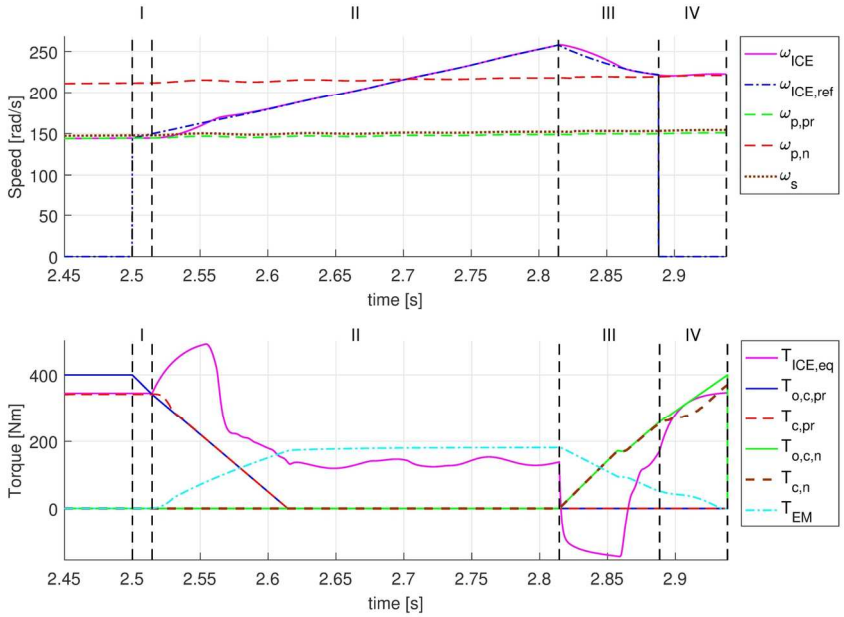

Figure 9. Speed and torque: 4th to 3rd at 100% APP: (a) AMT; (b) DCT

158x102mm (300 x 300 DPI)

Review

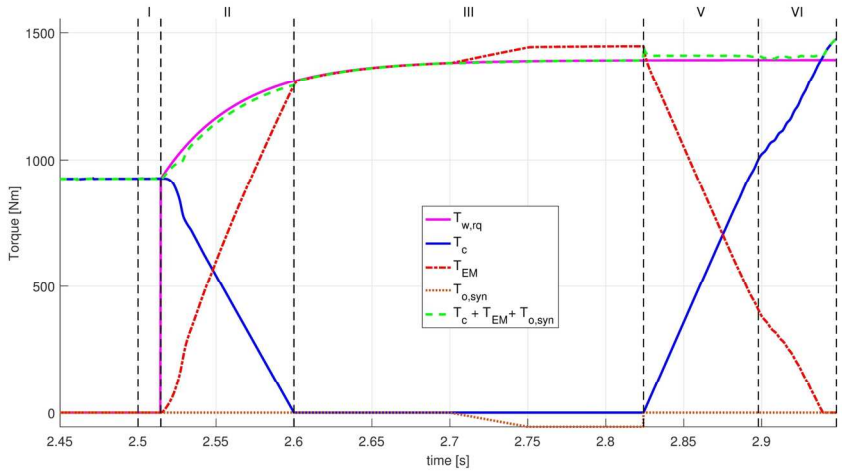

Figure 10. Torque at the wheels: 4th to 3rd at 100% APP: (a) AMT; (b) DCT

158x79mm (300 x 300 DPI)

eer Review

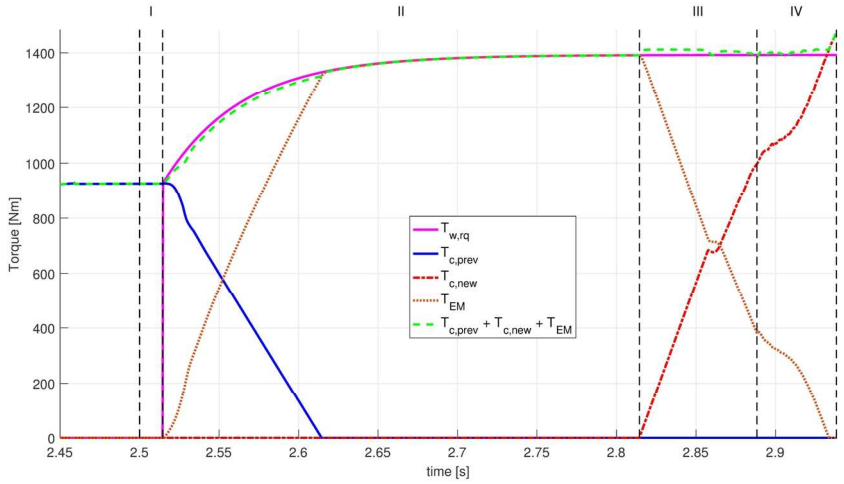

Figure 10. Torque at the wheels: 4th to 3rd at 100% APP: (a) AMT; (b) DCT

158x79mm (300 x 300 DPI)

eer Review

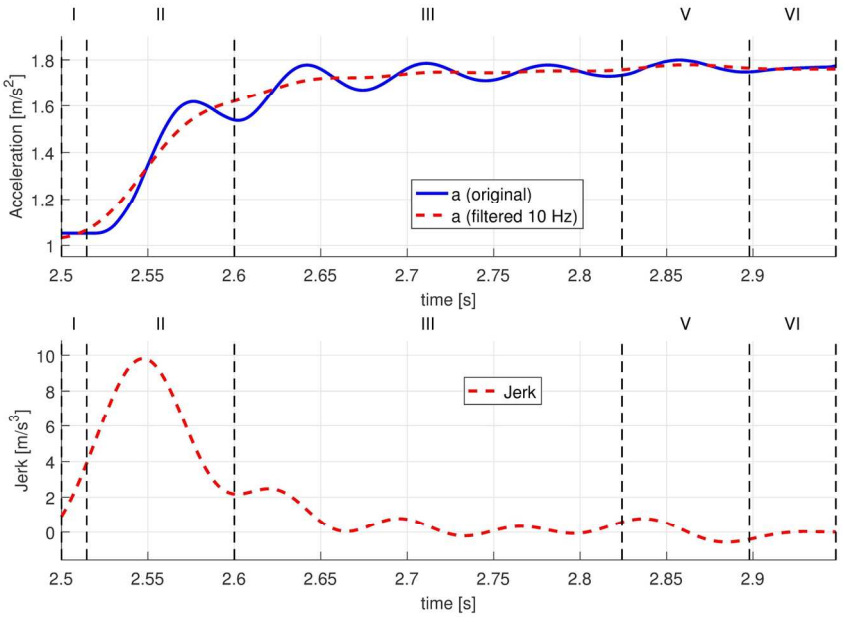

Figure 11. Acceleration and Jerk: 4th to 3rd at 100% APP: (a) AMT; (b) DCT

158x102mm (300 x 300 DPI)

Review

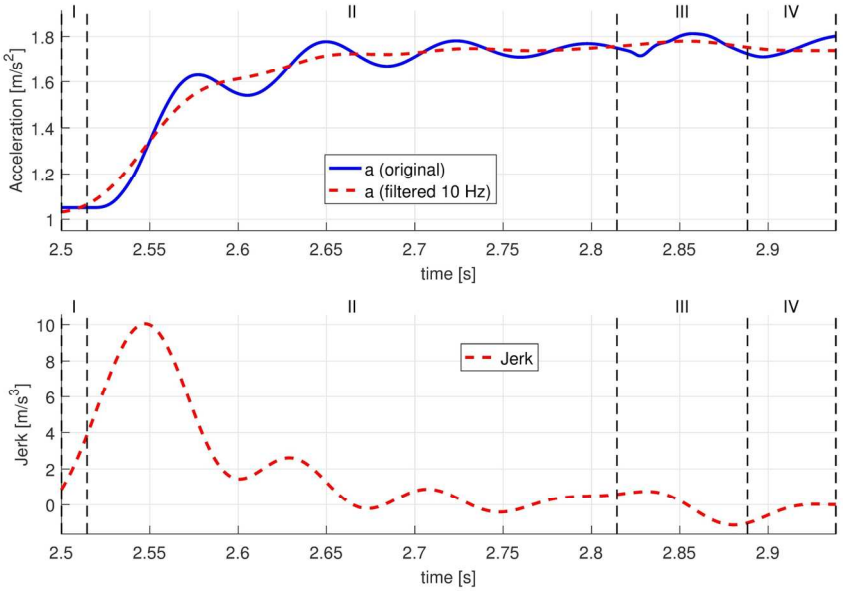

Figure 11. Acceleration and Jerk: 4th to 3rd at 100% APP: (a) AMT; (b) DCT

158x102mm (300 x 300 DPI)

Review